Scientific Research Publishing

Circuits and Systems, 2025, 16(3), 49-64
https://www.scirp.org/journal/cs
ISSN Online: 2153-1293
ISSN Print: 2153-1285

PWM-Based Current-Sensorless Adaptive Sliding-Mode Control for the Boost Converter with Constant Power Load

Said Oucheriah, Abul Azad

Department of Engineering Technology, Northern Illinois University, DeKalb, IL, USA
Email: soucheria@niu.edu, aazad@niu.edu

How to cite this paper: Oucheriah, S. and Azad, A. (2025) PWM-Based Current-Sensorless Adaptive Sliding-Mode Control for the Boost Converter with Constant Power Load. *Circuits and Systems*, **16**, 49-64.
https://doi.org/10.4236/cs.2025.163003

Received: February 16, 2025
Accepted: March 28, 2025
Published: March 31, 2025

Abstract

The boost converter feeding a constant power load (CPL) is a non-minimum phase system that is prone to the destabilizing effects of the negative incremental resistance of the CPL and presents a major challenge in the design of stabilizing controllers. Numerous studies in the design of stabilizing controllers have been proposed with the overwhelming majority of them requiring measurements of the inductor current for their implementation. To the best knowledge of the authors, very few studies in the literature have dealt with current-sensorless control of the DC-DC boost converters with CPL. In this work, a simple adaptive controller that relies only on the output voltage measurements for its design and implementation is introduced. A Luenberger-type observer is developed to estimate the inductor current and the output load power. A linear sliding surface is used to derive the controller that is simple in its design and yet exhibits excellent features in terms of robustness to external disturbances, parameter uncertainties, and parasitics. Also, a simple procedure to select the controller gains is outlined. The robustness of the controller is validated by computer simulations.

Keywords

Boost Converter, Robust Sliding Mode Control, Constant Power Load (CPL) and Current-Sensorless Control

1. Introduction

Nowadays, power electronic converters are extensively used in power distribution systems and are usually cascaded. Some of these converters operate as tightly

regulated loads that absorb constant power and behave as constant power loads (CPLs). These loads exhibit negative incremental impedances that can lead to serious destabilizing effects of the input sources, which may be other DC-DC converters and they present major challenges in the design of stabilizing robust controllers for the supply converters.

Numerous design techniques [1]-[13] and the references therein have been published in the literature to regulate the output voltage of DC-DC converters to counter the instability effects of the CPL-induced negative impedance. In these studies, the controllers require the measurements of the inductor currents in their implementations, which can be a challenging task in a noisy environment subject to large external disturbances. This situation has led to an interest in the use of current-sensorless controllers that may also reduce the cost and improve the reliability and miniaturization of the devices. In the context of the DC-DC boost converter feeding a CPL, very few studies appeared in the literature that deal with current-sensorless control.

In [14] and [15], a generalized parameter estimation is developed to estimate the inductor current and the unknown CPL of the converter based on dynamic regressor extension and mixing techniques. An adaptive sensorless-control scheme is achieved by incorporating these estimates into a full state feedback controller. The parameter estimators seem very complicated, with few details about their implementations. In [16], a PWM-based current-sensorless robust sliding mode controller is developed that requires only the measurement of the output voltage. A simple extended state observer is developed to estimate a lumped uncertainty signal that comprises the uncertain load power and the input voltage, the converter parasitics, the component uncertainties and the estimation of the derivative of the output voltage needed in the implementation of the controller. A linear sliding surface is used to derive a simple control law.

In this work, an estimator is developed to accurately estimate the unknown inductor current and the unknown CPL. Using these estimates, a simple control law is developed and a systematic procedure is proposed to select the adaptive controller gains. The effectiveness of the proposed adaptive controller is validated using simulations.

2. Boost Converter Averaged Model

A basic boost converter feeding a CPL is shown in **Figure 1**.

Under continuous conduction mode (CCM), the averaged model of the boost converter is

$$\begin{aligned} \dot{x}_1 &= -\frac{R_L}{L}x_1 - (1-u)\frac{x_2}{L} + \frac{E}{L} \\ \dot{x}_2 &= (1-u)\frac{x_1}{C} - \frac{P}{Cx_2} \end{aligned} \tag{1}$$

where x_1 represents the average inductor current and $x_2 \in \mathbb{R} > 0$ is the average output voltage. The parameters R_L, E, L, C and P represent the inductor

equivalent series resistance, the input voltage, the inductance, the capacitance and the load power respectively. The control input u to the converter is the duty ratio function. During the start-up phase diode D_1 guarantees that the initial condition

$$x_2(0) = E \tag{2}$$

with a reduction of the inrush current in the inductor [6]. Equation (2) ignores the parasitics and the conducting voltage of the diode D_1.

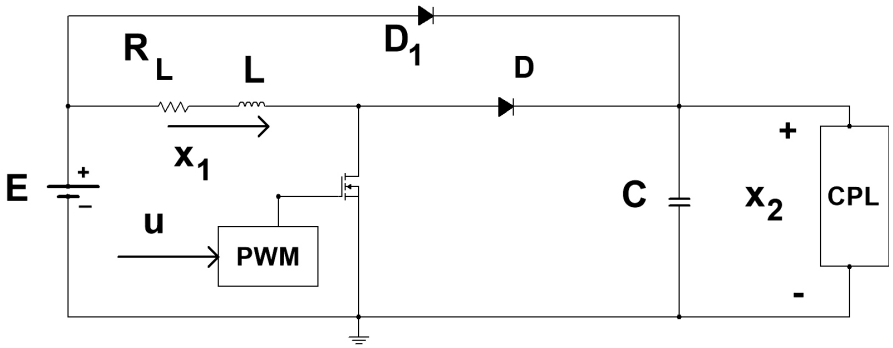

Figure 1. A boost converter feeding a CPL.

3. Current-Sensorless Adaptive Sliding Mode Control Design

3.1. Estimator and Adaptation Law

An estimator is used to estimate the inductor current and facilitate the design of the parameter adaptation law for the estimate of P. To this end, the following estimator is considered.

$$\begin{aligned} \dot{\hat{x}}_1 &= -\frac{R_L}{L}\hat{x}_1 - (1-u)\frac{\hat{x}_2}{L} + \frac{E}{L} \\ \dot{\hat{x}}_2 &= (1-u)\frac{\hat{x}_1}{C} - \frac{\hat{P}}{Cx_2} + K_2(x_2 - \hat{x}_2) \end{aligned} \tag{3}$$

where $\hat{x}_1, \hat{x}_2$ and $\hat{P}$ are the estimates of x_1, x_2 and P respectively with $K_2 > 0$ the estimator gain. Let $\tilde{x}_1 = x_1 - \hat{x}_1$, $\tilde{x}_2 = x_2 - \hat{x}_2$ and $\tilde{P} = P - \hat{P}$ then using (1) and (3), we obtain the following error equations

$$\begin{aligned} \dot{\tilde{x}}_1 &= -\frac{R_L}{L}\tilde{x}_1 - (1-u)\frac{\tilde{x}_2}{L} \\ \dot{\tilde{x}}_2 &= (1-u)\frac{\tilde{x}_1}{C} - \frac{\tilde{P}}{Cx_2} - K_2\tilde{x}_2 \end{aligned} \tag{4}$$

To generate the adaptation law for the estimate of P, we consider the following quadratic Lyapunov function

$$V = \frac{1}{2}L\tilde{x}_1^2 + \frac{1}{2}C\tilde{x}_2^2 + \frac{1}{2\gamma_p}\tilde{P}^2 \tag{5}$$

where $\gamma_p > 0$ is a design parameter. Its time derivative along the solutions of (4) is

$$\dot{V} = -R_L \tilde{x}_1^2 - K_2 C \tilde{x}_2^2 - \tilde{P}\left[\frac{\tilde{x}_2}{x_2} + \frac{\dot{\hat{P}}}{\gamma_p}\right] \tag{6}$$

The adaptation law is determined by cancelling the term in brackets and is given by

$$\dot{\hat{P}} = -\gamma_p \frac{\tilde{x}_2}{x_2} \tag{7}$$

With the adaptation law (7), we now have

$$\dot{V} = -R_L \tilde{x}_1^2 - K_2 C \tilde{x}_2^2 \tag{8}$$

Using Lasalle invariant principle, we can conclude that $\tilde{x}_1 \to 0, \tilde{x}_2 \to 0$ aymptotically. Since $\tilde{P} \to 0$ we have $\hat{P} \to P$.

3.2. Control Law Design

We consider the following switching surface

$$\sigma = \hat{x}_1 - \beta + K_d z_2 \tag{9}$$

where

$$\begin{aligned} \beta &= \frac{E - \sqrt{E^2 - 4R_L \hat{P}}}{2R_L} \\ z_2 &= \hat{x}_2 - V_{ref} \end{aligned} \tag{10}$$

The controller u is derived by differentiating σ with respect to time and setting $\dot{\sigma} = 0$. Using (3), (9) and (10), the control is given by

$$\begin{aligned} u = &\frac{C\hat{x}_2 + \left(R_L C - K_d L\right)\hat{x}_1 - EC + LC\dot{\beta} + \dfrac{K_d L \hat{P}}{x_2}}{C\hat{x}_2 - K_d L \hat{x}_1} \\ &- \frac{K_2 K_d L C \tilde{x}_2}{C\hat{x}_2 - K_d L \hat{x}_1} - \frac{K_s \sigma}{C\hat{x}_2 - K_d L \hat{x}_1} \end{aligned} \tag{11}$$

where

$$\dot{\beta} = \frac{\dot{\hat{P}}}{\sqrt{E^2 - 4R_L \hat{P}}} \tag{12}$$

The last term of the controller u given by (11) is added to ensure the sliding mode condition.

The substitution of the controller (11) into the derivative of (9) leads to

$$\dot{\sigma} = -K_s \sigma \tag{13}$$

and therefore we have $\dot{\sigma}\sigma = -K_s \sigma^2 < 0$, which ensures the sliding mode condition. Equation (13) admits as a solution

$$\sigma(t) = \sigma(0) \mathrm{e}^{-K_s t} \tag{14}$$

For a choice of the initial condition of the adaptation law $\hat{P}(0)$, the initial conditions of the estimator $\hat{x}_1(0)$ and $\hat{x}_2(0)$ are selected to guarantee the occurrence of sliding mode at $t = 0$ with the reaching phase completely eliminated with

$$\begin{aligned}\hat{x}_2(0) &= V_{ref}\\ \beta(0) &= \frac{E-\sqrt{E^2-4R_L\hat{P}(0)}}{2R_L}\\ \hat{x}_1(0) &= \beta(0)\end{aligned} \tag{15}$$

This yields $\sigma(0)=0$ and in view of (14), $\sigma(t)=0$ for all $t\geq 0$. In this case we have

$$\hat{x}_1(t) = \beta - K_d z_2(t),\ t\geq 0 \tag{16}$$

3.3. Adaptive Controller Gains and Stability

The parasitics of the converter increase the natural damping of the system [1], [17] and reduce the destabilizing effect of the CPL. Therefore, we set $R_L = 0\,\Omega$ for which the destabilizing effect are more pronounced for the stability analysis.

For $R_L = 0\,\Omega$ we consider $\beta = \frac{\hat{P}}{E}$. Using (7), $\dot{\beta} = \frac{\dot{\hat{P}}}{E} = -\gamma_p \frac{\tilde{x}_2}{Ex_2}$ and equation (16) becomes

$$\hat{x}_1(t) = \frac{\hat{P}}{E} - K_d z_2(t),\ t\geq 0 \tag{17}$$

Substituting the controller (11) into the second equation of (3) and using (17) with $\sigma = 0$ yields the following equation

$$\dot{\hat{x}}_2 = \frac{\left[EC - \frac{\hat{P}LK_d}{x_2}\right]\left[\frac{\hat{P}}{EC} - \frac{K_d z_2}{C}\right]}{C\hat{x}_2 - K_d L\left(\frac{\hat{P}}{E} - K_d z_2\right)} - \frac{\hat{P}}{Cx_2} + \Psi_1 \tag{18}$$

where

$$\Psi_1 = \frac{L\gamma_p \frac{\hat{x}_1\tilde{x}_2}{Ex_2} + K_2K_dL\hat{x}_1\tilde{x}_2}{C\hat{x}_2 - K_dL\left(\frac{\hat{P}}{E} - K_d z_2\right)} + K_2\tilde{x}_2 \tag{19}$$

Multiplying both sides of (18) by the denominator $C\hat{x}_2 - K_dL\left(\frac{\hat{P}}{E} - K_d z_2\right)$ yields

$$\dot{\hat{x}}_2\left[C\hat{x}_2 - K_dL\left(\frac{\hat{P}}{E} - K_d z_2\right)\right] = -K_dEz_2 + \Psi_2 \tag{20}$$

where

$$\Psi_2 = \Psi_1\left[C\hat{x}_2 - K_dL\left(\frac{\hat{P}}{E} - K_d z_2\right)\right] + \frac{\hat{P}}{x_2}\tilde{x}_2 \tag{21}$$

Using $\dot{\hat{x}}_2 = \dot{z}_2$ and $z_2 = \hat{x}_2 - V_{ref}$ we can write (20) as

$$\begin{aligned} & C\dot{z}_2\left[z_2+V_{ref}\right]-K_dL\dot{z}_2\left[\frac{\hat{P}}{E}-K_dz_2\right] \\ & =\dot{z}_2\left[\left(C+K_d^2L\right)z_2+\left(CV_{ref}-K_dL\frac{\hat{P}}{E}\right)\right] \\ & =-K_dEz_2+\Psi_2 \end{aligned} \tag{22}$$

and

$$\dot{z}_2=\frac{-K_dEz_2+\Psi_2}{\left(C+K_d^2L\right)z_2+CV_{ref}-K_dL\dfrac{\hat{P}}{E}} \tag{23}$$

Since $\tilde{x}_2\to 0$, $\Psi_1\to 0$ and therefore $\Psi_2\to 0$. For $K_d>0$ we want the denominator of (23) to be positive to establish stability. Using $z_2=\hat{x}_2-V_{ref}$ we want

$$\left(C+K_d^2L\right)\left(\hat{x}_2-V_{ref}\right)+CV_{ref}-K_dL\frac{\hat{P}}{E}>0 \tag{24}$$

The crucial case in satisfying condition (24) is when $\hat{x}_2<V_{ref}$ starting with $\hat{x}_2(0)=V_{ref}$ since the first term and the last term of (24) are both negative. This situation occurs with the existence of undershoots with the maximum possible magnitude undershoot $\hat{x}_2(\min)=pV_{ref}$, $0<p<1$. The first undershoot being the most critical in the determination of K_d for stability as subsequent undershoots, if they exist, will be decreasing since Ψ_2 is decreasing with time as $\tilde{x}_2\to 0$. In this case, it will be shown that there exist a gain K_d such that condition (24) is satisfied for all $t\geq 0$ and asymptotic stability is achieved with $z_2\to 0$, $\hat{x}_2\to V_{ref}$ and $x_2\to V_{ref}$. From (17) $\hat{x}_1\to\dfrac{P}{E}$ and $x_1\to\dfrac{P}{E}$ since $\tilde{x}_1\to 0$.

Assume that $\hat{x}_2(t)$ undershoots to $\hat{x}_2(\min)=pV_{ref}$, $0<p<1$. The worst case for condition (24) to hold is when $\hat{P}=\hat{P}_{\max}$ and in this case condition (24) becomes

$$\left(C+K_d^2L\right)\left(\hat{x}_2-V_{ref}\right)+\left(CV_{ref}-K_dL\frac{\hat{P}_{\max}}{E}\right)>0 \tag{25}$$

Substituting $\hat{x}_2=pV_{ref}$, condition (25) is written as

$$K_d^2LV_{ref}\left(p-1\right)-K_dL\frac{\hat{P}_{\max}}{E}+CpV_{ref}>0 \tag{26}$$

The quadratic equation in K_d given by (26) admits two roots $K_{d_1}<0$ and $K_{d_2}>0$ with

$$\begin{aligned} K_{d_1} &= \frac{\dfrac{L\hat{P}_{\max}}{E}+\sqrt{\left(\dfrac{L\hat{P}_{\max}}{E}\right)^2-4L\left(p-1\right)V_{ref}^2pC}}{2L\left(p-1\right)V_{ref}} \\ K_{d_2} &= \frac{\dfrac{L\hat{P}_{\max}}{E}-\sqrt{\left(\dfrac{L\hat{P}_{\max}}{E}\right)^2-4L\left(p-1\right)V_{ref}^2pC}}{2L\left(p-1\right)V_{ref}} \end{aligned} \tag{27}$$

For the condition (26) to be satisfied the gain $K_d > 0$ should be chosen as

$$0 < K_d < K_{d_2} \tag{28}$$

and (26) is satisfied for $\hat{x}_2(t) \geq pV_{ref}$, $0 < p < 1$.

It is straightforward to show that K_d given by (28) will also satisfy condition (25) for the case of an overshoot of $\hat{x}_2$. Therefore, for $\hat{x}_2 \geq pV_{ref}$, $p > 0$ condition (25) is satisfied and asymptotic stability is achieved with $x_2 \to V_{ref}$, $\hat{P} \to P$ and finally $x_1 \to \frac{P}{E}$.

Remark 1: The determination of the gain K_d depends on the knowledge of $\hat{x}_2(\min)$. The auxiliary diode D_1 constrains the output x_2 to

$$x_2 = \hat{x}_2 + \tilde{x}_2 \geq E \tag{29}$$

From (23) to ensure that the estimator has much faster dynamics than the controlled feedback system, the gain of the estimator K_2 must be chosen much greater than $K_d E$ to ensure that $\tilde{x}_2 \to 0$ at a much faster rate than the controlled output to V_{ref}. Please also note that initially we have $x_2(0) = E$ and $\hat{x}_2(0) = V_{ref}$. In this case, we can assume that the maximum possible undershoot of $\hat{x}_2$ is constrained to

$$\hat{x}_2(\min) = E \tag{30}$$

Remark 2: A possible general guideline for the choice of the controller and estimator gains is:

1) Choose $K_s = 1$ to satisfy the sliding mode condition. Choose a high gain γ_p for the adaptation law (7). The higher the gain, the faster the convergence of the estimated $\hat{P}$ to the actual P. However, if the gain is too high, there will be small oscillations in the output response during load power disturbances.

2) Choose $\hat{x}_2(0) = V_{ref}$ and a value for $\hat{P}(0)$ and determine $\hat{x}_1(0)$ given by (15) to guarantee that the sliding mode starts at $t = 0$ s with the reaching phase completely eliminated.

3) Choose $\hat{P}_{\max}$ to be 3 to 5 greater than the expected maximum load power P.

4) As discussed previously, the crucial factor that determines the stability of the closed-loop system is the existence of an undershoot of maximum amplitude $\hat{x}_2(\min) = pV_{ref} = E$. In this case, we have

$$p = \frac{E}{V_{ref}} \tag{31}$$

5) Calculate K_{d_2} using (27) and choose the gain K_d to be

$$K_d = K_d^* = 0.5K_{d_2} \tag{32}$$

In this case, the maximum possible magnitude of the undershoot $\hat{x}_2(\min) = p_1 V_{ref}$ with $p_1 < p$ for which stability is maintained is determined by p_1 given by

$$p_1 = \frac{K_d^{*2} L V_{ref} + \dfrac{K_d^* L P_{\max}}{E}}{K_d^{*2} L V_{ref} + C V_{ref}} \tag{33}$$

6) In view of Remark 1, choose the gain of the estimator $K_2 = 50 \times m \times K_d E$ with $m \geq 1$ to ensure that the estimator has faster dynamics than the controlled feedback system.

Shown in Figure 2 is the block diagram of the proposed controlled system.

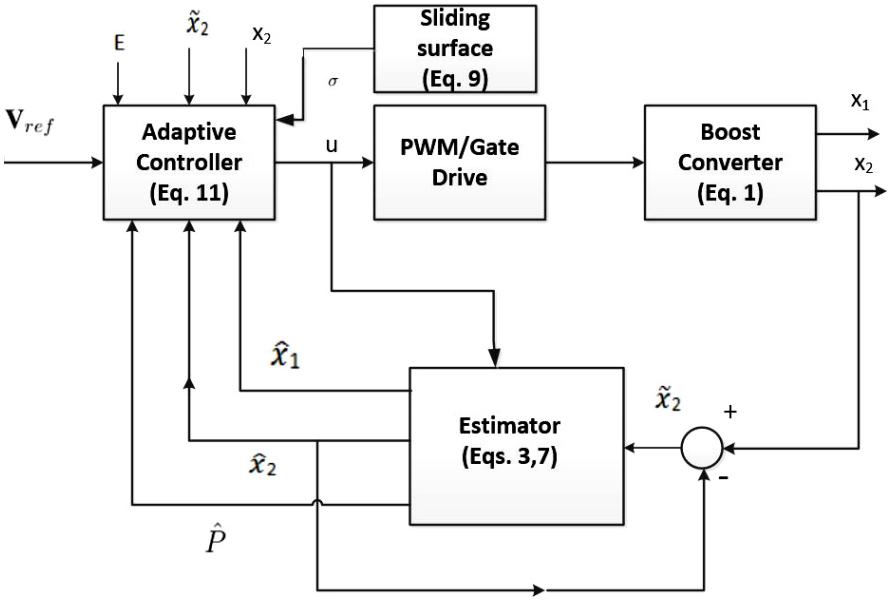

Figure 2. Block diagram of the proposed controlled system.

4. Simulation Results

The nominal DC-DC boost converter parameters that are used for the comparaison simulations are the ones used in [15] and they are

$$L_o = 330\ \mu\text{H},\ C_o = 820\ \mu\text{F},\ P_o = 30\ \text{W},\ E_o = 15\ \text{V},\ V_{ref} = 25\ \text{V} \tag{34}$$

The simulations are performed using the averaged model (1).

For robustness to parameter uncertainties, the actual parameters of the converters that are unknown to the designers are

$$L = (1 \pm 30\%) L_o,\ \ C = (1 \pm 30\%) C_o \tag{35}$$

In [15], the parameter uncertainties considered are ±10%.

To account for the conduction losses, we consider the inductor equivalent series resistance R_L and the capacitor equivalent series resistance R_C as in [15] and they are

$$R_L = 0.2\ \Omega,\ \ R_C = 0.3\ \Omega \tag{36}$$

Using the guideline in Remark 2 with

$$\gamma_p = 1 \times 10^6,\ m = 10,\ \hat{P}(0) = 0\ \text{W},\ P_{\max} = 120\ \text{W} \tag{37}$$

we have

$$K_s = 1,\ p = 0.6,\ K_d = 0.7860,\ K_2 = 5.894\times 10^3,\ p_1 = 0.28 \tag{38}$$

Case 1: In this case we consider the actual inductance and capacitance have increased by 30% from their nominal values with the converter subjected to step load power changes from 30 W to 25 W at $t = 0.1\,\text{s}$ and from 25 W to 30 W at $t = 0.2\,\text{s}$. Figure 3 depicts the output voltage response of the converter with the proposed controller exhibiting an excellent power disturbance suppression capability with very small overshoots/undershoots and short recovery times.

Figures 4-7 represent the inductor current x_1 and its estimate $\hat{x}_1$, the current estimation error $\tilde{x}_1$, the load power P and its estimate $\hat{P}$ and the load power estimation error $\tilde{P}$, respectively. Despite the parasitics and the large parameter uncertainties, the steady-state errors in the output voltage and the estimates are zero. The plot of the duty ratio function u is shown in Figure 8.

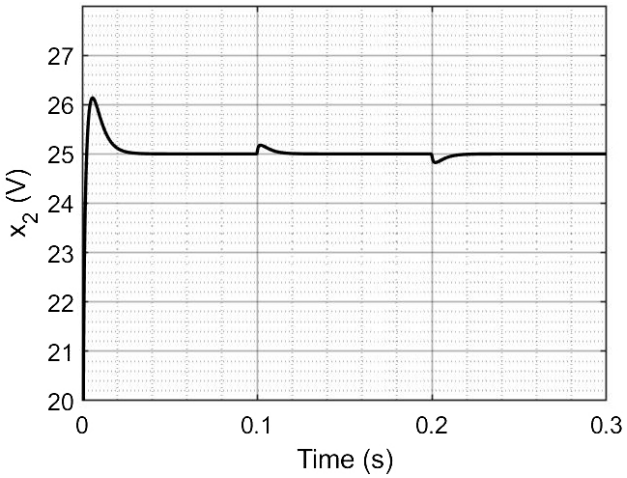

Figure 3. Case 1: Output voltage responses for a power load step change from 30 W to 25 W at $t = 0.1\,\text{s}$ and from 25 W to 30 W at $t = 0.2\,\text{s}$ with an increse in inductance and capacitance by 30%.

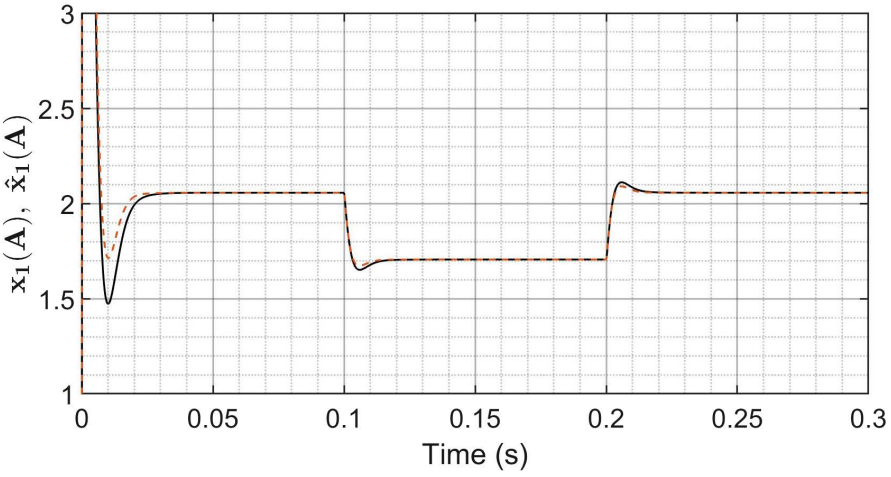

Figure 4. Case 1: Current x_1 in black and its estimate $\hat{x}_1$ in red.

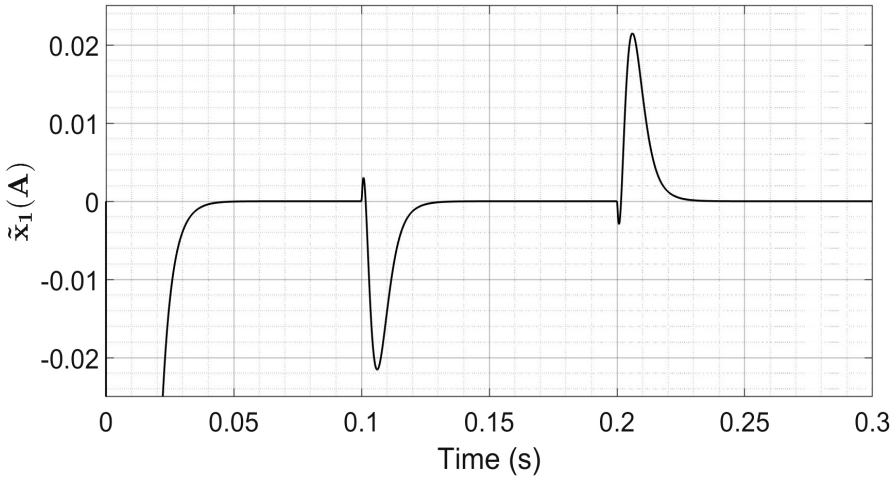

Figure 5. Case 1: Current estimation error $\tilde{x}_1$.

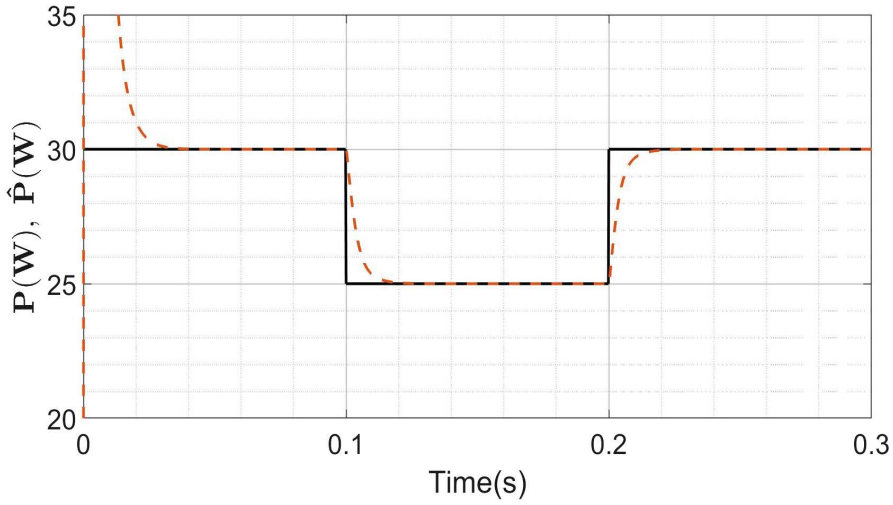

Figure 6. Case 1: Load power P in black and its estimate $\hat{P}$ in red.

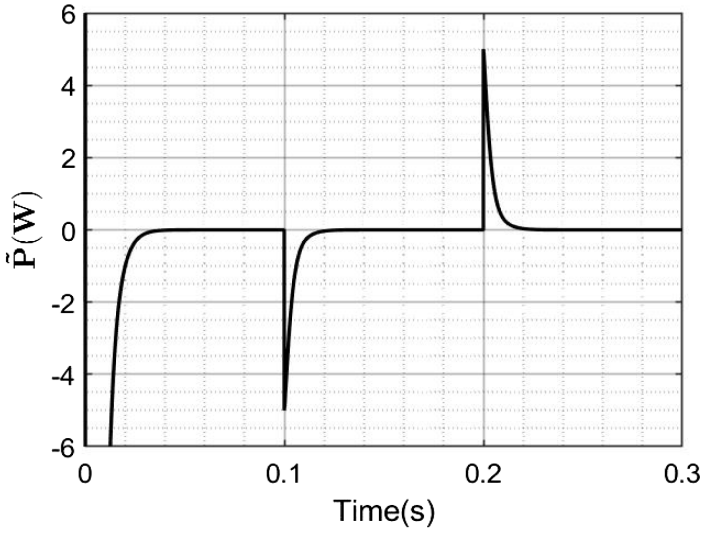

Figure 7. Case 1: Load power estimation error $\tilde{P}$.

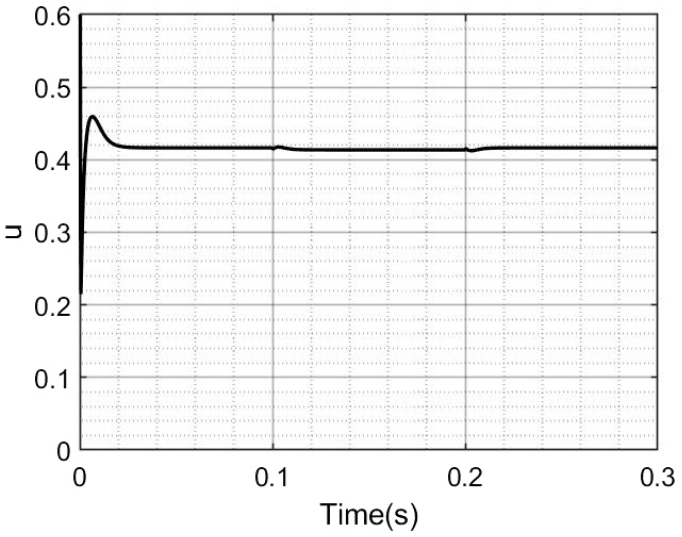

Figure 8. Case 1: Duty ratio function u.

Case 2: Same conditions as in Case 1 but with a decrease in the values of the actual inductance and capacitance by 30% from their nominal values. Figure 9 depicts the output response with Figure 10 and Figure 11 representing the current estimation error $\tilde{x}_1$ and the load power estimation error $\tilde{P}$ respectively for the proposed controller. As in Case 1, the adaptive controller achieved a high performance in term of load power disturbance rejection capability with perfect tracking of the reference voltage and accurate estimations of the inductor current and the load power.

Case 3: Keeping the same inductance and capacitance as in Case 1, here the converter is subjected to a time-varying load power P shown in Figure 12 with its estimate $\hat{P}$. Figure 13 depicts the output response. For the case of step-load power changes, the output voltage tightly tracks the reference voltage with zero

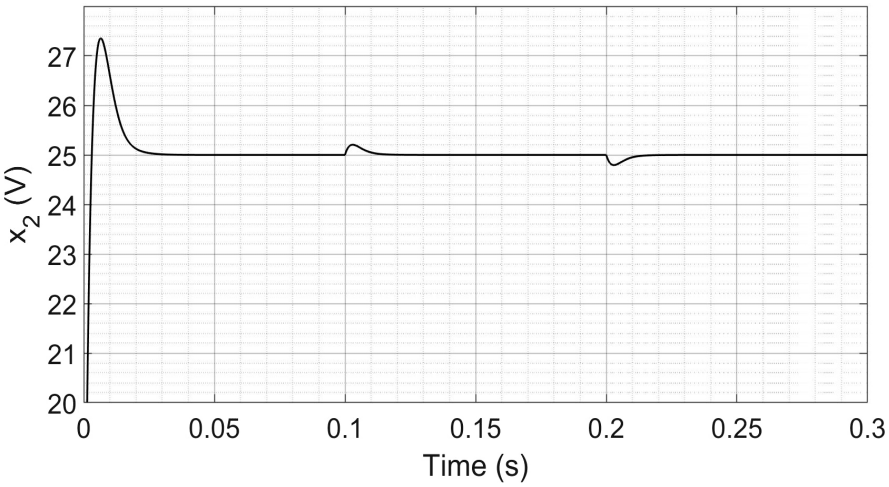

Figure 9. Case 2: Output voltage response for a power load step change from 30 W to 25 W at $t = 0.1\,\text{s}$ and from 25 W to 30 W at $t = 0.2\,\text{s}$ with a decrease in inductance and capacitance by 30%.

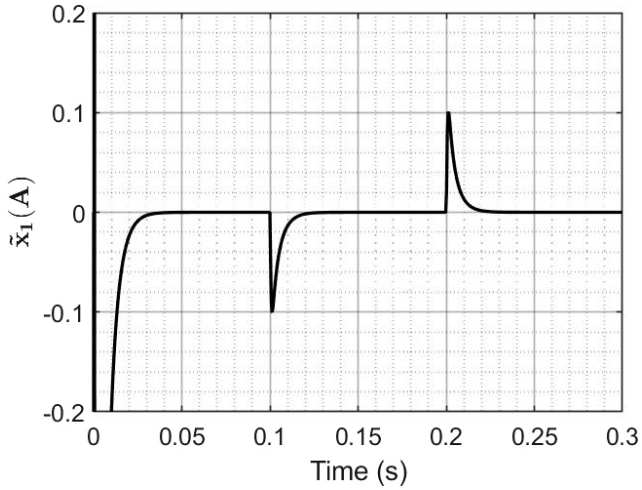

Figure 10. Case 2: Current estimation error $\tilde{x}_1$.

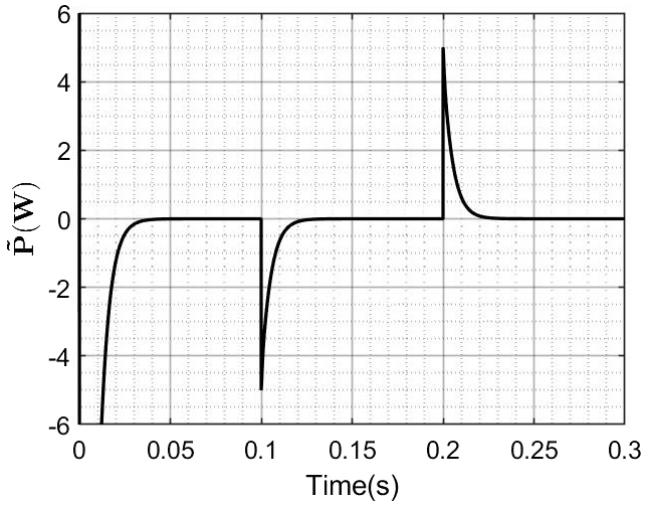

Figure 11. Case 2: Load power estimation error $\tilde{P}$.

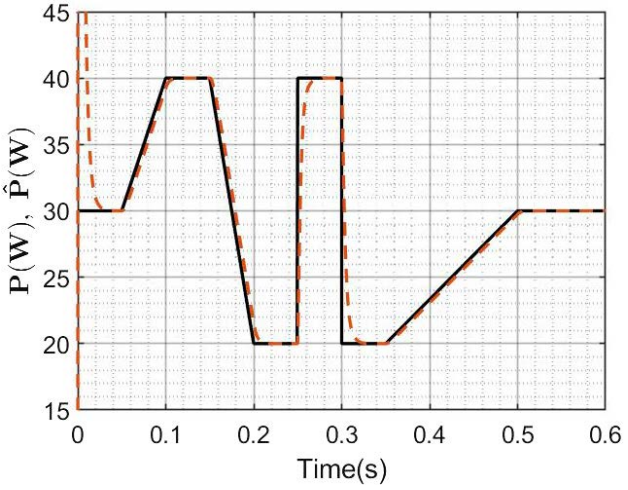

Figure 12. Case 3: Time-varying power P in black and its estimate $\hat{P}$ in red.

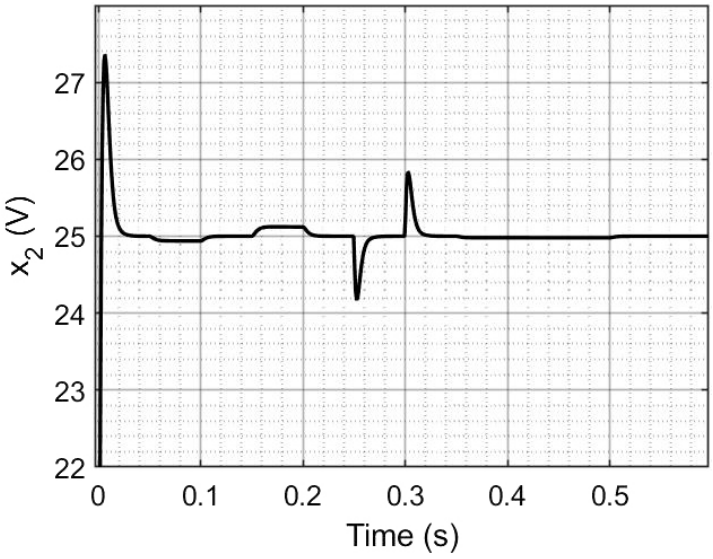

Figure 13. Case 3: Output voltage responses for the time-varying load power shown in **Figure 12**.

steady-state errors. However, in the case of slowly time-varying load power, there will be steady-state errors in the output voltage with a maximum of 120 mV. Small offset errors are also present in the estimations of the inductor current and load power. **Figures 14-16** represent the load power estimation error $\tilde{P}$, the inductor current x_1 and its estimate $\hat{x}_1$ and the current estimation error $\tilde{x}_1$, respectively.

Case 4: Same conditions as in Case 1 but with two different inductor parasitics. Shown in **Figure 17** is the output responses for $R_L = 0.1\,\Omega$ in red and $R_L = 0.3\,\Omega$ in black. Both are the actual inductor equivalent series resistances that are unknown to the designer. The proposed controller is designed based on the nominal value of $R_L = 0.2\,\Omega$. As seen in the plots, both output voltage responses tightly track the reference voltage with zero steady-state errors.

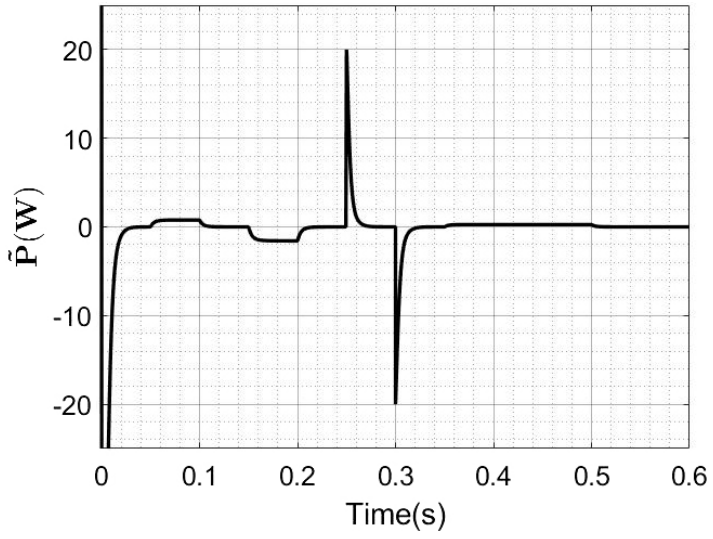

Figure 14. Case 3: Load power estimation error $\tilde{P}$.

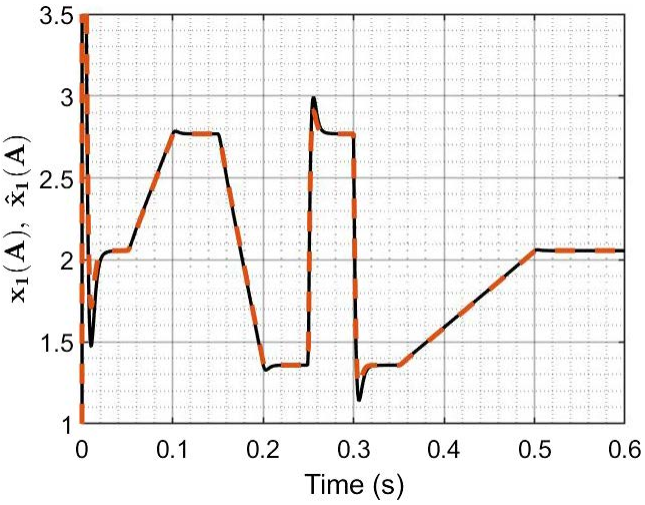

Figure 15. Case 3: Current x_1 in black and its estimate $\hat{x}_1$ in red.

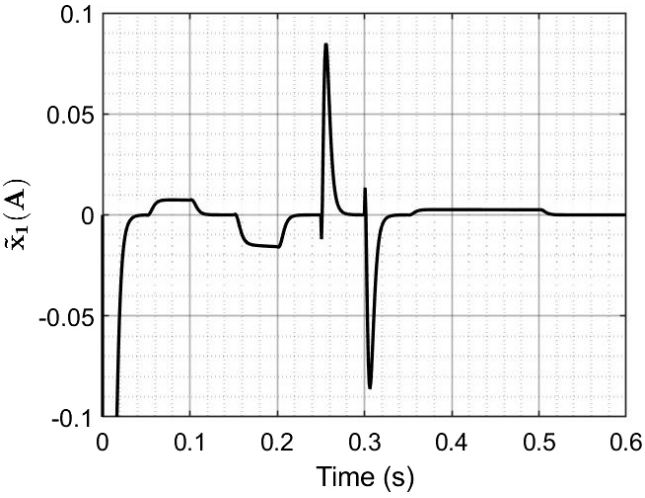

Figure 16. Case 3: Current estimation error $\tilde{x}_1$.

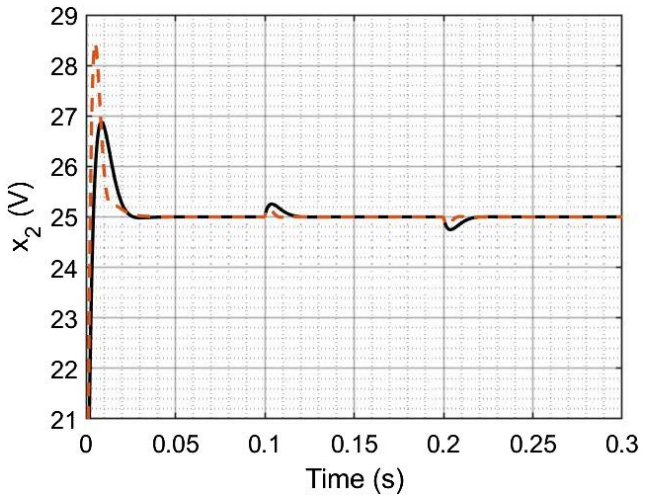

Figure 17. Case 4: Output voltage response for $R_L = 0.1\,\Omega$ in red and $R_L = 0.3\,\Omega$ in black.

5. Conclusion

A Luenberger-type observer is used to accurately estimate the unknown load power and the inductor current. A linear sliding surface is used to derive a simple adaptive controller. A systematic procedure is developed to determine the controller and estimator gains. The robustness of the proposed controller is validated with simulations. Future work will be the validation of the controller experimentally.

Conflicts of Interest

The authors declare that there is no competing financial interest that could have appeared to influence the work reported in this paper.

References

[1] Singh, S., Rathore, N. and Fulwani, D. (2016) Mitigation of Negative Impedance Instabilities in a DC/DC Buck-Boost Converter with Composite Load. *Journal of Power Electronics*, **16**, 1046-1055. https://doi.org/10.6113/jpe.2016.16.3.1046

[2] He, W., Ortega, R., Machado, J.E. and Li, S. (2018) An Adaptive Passivity-Based Controller of a Buck-Boost Converter with a Constant Power Load. *Asian Journal of Control*, **21**, 581-595. https://doi.org/10.1002/asjc.1751

[3] He, W., Soriano-Rangel, C.A., Ortega, R., Astolfi, A., Mancilla-David, F. and Li, S. (2018) Energy Shaping Control for Buck-Boost Converters with Unknown Constant Power Load. *Control Engineering Practice*, **74**, 33-43. https://doi.org/10.1016/j.conengprac.2018.02.006

[4] Martinez-Trevino, B.A., El Aroudi, A., Vidal-Idiarte, E., Cid-Pastor, A. and Martinez-Salamero, L. (2019) Sliding-Mode Control of a Boost Converter under Constant Power Loading Conditions. *IET Power Electronics*, **12**, 521-529.

[5] Soriano-Rangel, C.A., He, W., Mancilla-David, F. and Ortega, R. (2021) Voltage Regulation in Buck-Boost Converters Feeding an Unknown Constant Power Load: An Adaptive Passivity-Based Control. *IEEE Transactions on Control Systems Technology*, **29**, 395-402. https://doi.org/10.1109/tcst.2019.2959535

[6] Martinez-Trevino, B.A., Aroudi, A.E., Valderrama-Blavi, H., Cid-Pastor, A., Vidal-Idiarte, E. and Martinez-Salamero, L. (2021) PWM Nonlinear Control with Load Power Estimation for Output Voltage Regulation of a Boost Converter with Constant Power Load. *IEEE Transactions on Power Electronics*, **36**, 2143-2153. https://doi.org/10.1109/tpel.2020.3008013

[7] Riffo, S., Gil-González, W., Montoya, O.D., Restrepo, C. and Muñoz, J. (2022) Adaptive Sensorless Pi+Passivity-Based Control of a Boost Converter Supplying an Unknown CPL. *Mathematics*, **10**, Article No. 4321. https://doi.org/10.3390/math10224321

[8] He, W. and Shang, Y. (2022) Finite-Time Parameter Observer-Based Sliding Mode Control for a DC/DC Boost Converter with Constant Power Loads. *Electronics*, **11**, Article No. 819. https://doi.org/10.3390/electronics11050819

[9] Oucheriah, S. (2022) Nonlinear Control of the Boost Converter Subject to Unknown Constant Power Load and Parasitics. *International Journal of Electronics Letters*, **11**, 30-40. https://doi.org/10.1080/21681724.2021.2025438

[10] Gil-González, W., Riffo, S., Montoya, O.D., Restrepo, C. and Hernández, J.C. (2023) Adaptive Voltage Control for Second-Order DC-DC Converters Supplying an Unknown Constant Power Load: A Generalized PBC Plus Damping Injection Design.

IEEE Access, **11**, 47390-47409. https://doi.org/10.1109/access.2023.3275083

[11] Abdolahi, M., Adabi, J. and Mousazadeh Mousavi, S.Y. (2024) Implementation and Control of a Buck-boost Converter Connected to a Constant Power Load in a DC Microgrid. *Electrical Engineering*, **107**, 1483-1492. https://doi.org/10.1007/s00202-024-02538-x

[12] Zambrano-Prada, D.A., Aroudi, A.E., López-Santos, O., Vázquez-Seisdedos, L. and Martí-Nez-Salamero, L. (2025) Adaptive Sliding Mode Control of a Boost Converter with Unknown Constant Power Load. *IEEE Access*, **13**, 33714-33732. https://doi.org/10.1109/access.2025.3543659

[13] Oucheriah, S. and Azad, A. (2024) Ude-Based Robust Nonlinear Control of the Boost Converter with Constant Power Load. *Circuits and Systems*, **15**, 57-71. https://doi.org/10.4236/cs.2024.155005

[14] Wang, X., He, W. and Li, T. (2023) An Adaptive Observer for Current Sensorless Control of Boost Converter Feeding Unknown Constant Power Load. *Proceedings of* 2023 *Chinese Intelligent Automation Conference*. *CIAC* 2023, Vol. 1082, 830-837. https://doi.org/10.1007/978-981-99-6187-0_83

[15] He, W., Wang, X., Namazi, M.M., Zhou, W. and Guerrero, J.M. (2024) A Reduced-Order Adaptive State Observer for DC-DC Converters with Unknown Constant Power Load. *Control Engineering Practice*, **143**, 105785. https://doi.org/10.1016/j.conengprac.2023.105785

[16] Oucheriah, S. and Azad, A. (2024) Robust Nonlinear Current Sensorless Control of the Boost Converter with Constant Power Load. *Circuits and Systems*, **15**, 29-43. https://doi.org/10.4236/cs.2024.153003

[17] Huddy, S.R. and Skufca, J.D. (2013) Amplitude Death Solutions for Stabilization of DC Microgrids with Instantaneous Constant-Power Loads. *IEEE Transactions on Power Electronics*, **28**, 247-253. https://doi.org/10.1109/tpel.2012.2196056